

## Contribution of $f$ -electron excitation to electronic stopping power of platinum for protons

Shi-Ming Li,<sup>1</sup> Fei Mao<sup>1,\*</sup>, Xu-Dong Zhao<sup>2</sup>, Wen-Qi Jin<sup>1</sup>, Wen-Qi Zuo,<sup>1</sup>  
Bing-Sheng Li<sup>3</sup>, Feng Wang,<sup>4</sup> and Feng-Shou Zhang<sup>5</sup>


<sup>1</sup>*School of Nuclear Science and Technology, University of South China, Hengyang 421001, China*

<sup>2</sup>*School of Physics and Electronics, Hunan University, Changsha 410082, China*

<sup>3</sup>*State Key Laboratory for Environment-Friendly Energy Materials, Southwest University of Science and Technology, Mianyang, Sichuan 621010, China*

<sup>4</sup>*School of Physics, Beijing Institute of Technology, Beijing 100081, China*

<sup>5</sup>*The Key Laboratory of Beam Technology of Ministry of Education, College of Nuclear Science and Technology, Beijing Normal University, Beijing 100875, China*

 (Received 4 May 2022; accepted 22 June 2022; published 7 July 2022; corrected 15 July 2022 and 18 July 2022)

The electronic stopping power of protons traveling along the channeling and off-channeling trajectories in platinum (Pt) is reported based on time-dependent density functional theory calculations for electrons combined with Ehrenfest molecular dynamics simulations for ions in real time and real space. We provided an intuitive description of the electronic stopping power for a wide range of ion energies, and revealed the excitation mechanism for the inner  $4f$  electrons of Pt. The comparison of calculation results with experimental data showed that conduction electrons are sufficient to describe the electronic stopping power of Pt accurately in the low-energy range. The excitation of  $4f$  electrons contributes substantially to the electronic stopping power of Pt as the proton velocity exceeds 1.0 a.u. Our calculated stopping power is in quantitative agreement with the experimental data up to the stopping maximum, and showed that the stopping power obtained from the off-channeling geometry is greatly improved in comparison with the channeling results. Finally, the velocity dependence of the mean steady-state charge of protons was quantified, and the results showed that the instantaneous charge state of protons exhibits periodic oscillations in the low-energy region, while the periodic oscillations disappears in the high-energy region due to more ionization of protons.

DOI: [10.1103/PhysRevB.106.014103](https://doi.org/10.1103/PhysRevB.106.014103)

### I. INTRODUCTION

The study of the interaction between ions and solids is an active field of fundamental science and represents a key quantity for manifold technological applications [1]. It has important applications in areas of ion implantation [2,3], nuclear engineering [4], radiation protection [5], and materials engineering for space electronics [6,7]. The energy loss of ions traveling through materials has been a subject of interest since the early days of nuclear physics and it is the starting basis for both detailed calculations and practical applications in ion-beam therapies [8,9]. The retarding force acting on energetic ions (projectiles) due to the interaction with the media, resulting in the energy loss of ions, is referred to as stopping power  $S$ .  $S$  is used as a basic quantity to characterize the energy loss of ions passing through substances. This force can be quantitatively described as the average energy deposited per unit distance by the ions to the host (target) materials, which is generally divided into two categories depending on the type of excitation produced: (i) elastic collisions between ions and host nuclei that cause displacement damage, referred to as nuclear stopping power  $S_n$  [10,11]; and (ii) inelastic collisions between ions and host electrons that lead to electronic excita-

tion and ionization, referred to as electronic stopping power  $S_e$ . The stopping power is a function of projectile velocity or energy, and it also depends on the type of ion and the properties of the materials.

The  $S_n$  is the primary energy loss channel at low ion velocities, while  $S_e$  is becoming dominant when the projectiles reach the Bohr velocity. Compared with the nuclear stopping, the electronic stopping presents additional challenges due to its quantum mechanical nature. Extensive experimental and theoretical studies were carried out on the electronic stopping of light ions in targets at a wide range of energies and reasonable results of the  $S_e$  behavior in various materials were obtained [12–19]. Although there is numerous research on the stopping of ions, many theoretical calculations [20,21] for the  $S_e$  of transition metals do not agree with the experimental data.

Free electron gas (FEG) theory [22] holds that the  $S_e$  is proportional to ion velocity in the low-energy region. This velocity dependence was verified experimentally in most metallic targets [23–26]. One of the most conspicuous aspects of the electronic energy loss of light ions is that the  $S_e$  deviates from the expected velocity proportionality for noble metals at low energies. Valdés *et al.* [27] proposed that the contribution of  $d$ -electron excitation is responsible for the deviations from the velocity proportionality of the measured  $S_e$  of copper, silver, and gold for slow protons. A large number of experiments and theoretical studies, such as real-time

\*Corresponding author: maofei@mail.bnu.edu.cn

time-dependent density functional theory (RT-TDDFT) [28], which shows many meaningful advantages in describing the excited electron dynamics under ion irradiation, reproduced the  $S_e$  deviates from velocity proportionality [29–31]. However, it was found that the  $S_e$  of Pt for protons exhibited the velocity proportionality which was consistent with the FEG prediction at low ion velocities [32].

At low velocities, it is necessary to consider the charge exchange contribution to the energy loss of ions. Wilhelm *et al.* [33] measured the energy loss of slow highly charged Xe ions transmitted through ultrathin carbon membranes and found that the electronic energy loss was strongly related to the charge loss and the incident charge state of ions. By quantifying the velocity-dependent steady-state charge of protons and  $\alpha$  particles from nonequilibrium simulations, the velocity regime within which the linear response treatment is appropriate for describing the  $S_e$  of silicon carbide [34] and liquid water [35] was examined. These results showed that the description of the charge exchange was required for a deeper understanding of the microcosmic mechanism for the energy loss of ions. Most theories similar to the FEG model do not consider the charge exchange between the projectile ions and the host atoms, which is becoming especially important at low velocities [32,33].

At higher velocities, the contribution of inner-shell electron excitation to  $S_e$  attracted much attention in recent years. In particular, the degree to which the medium- and high-energy  $S_e$  obtained from theoretical calculations is consistent with the experimental results or SRIM predictions [36] is dominated by whether sufficient core electrons are considered. Ojanperä *et al.* [37] calculated the electronic energy loss of energetic ions penetrating graphitic targets from first principles and proved that this approach provided an accurate description of  $S_e$  for many ions at a wide energy range; not only the valence electrons, but also the core electrons were essential for the high-energy  $S_e$ . Schleife *et al.* [38] reported the importance of the contribution of semicore electron excitation to the  $S_e$  and found a large fraction of the semicore electrons participated in the off-channeling stopping. The results also indicated great promise in applying the first-principles methodology for investigating important problems in materials under ion radiation, such as the role played by atomic defects in electron-ion energy transfer. The study of the  $S_e$  of nickel for protons and  $\alpha$  particles also suggested that the inner electrons of the host play an important role in the high-energy stopping power [39].

In recent years, the contribution of inner electrons to  $S_e$  is mainly focused on the study of  $d$ -electron excitation. For transition metals within period 6, measurements showed that  $4f$  electrons play a crucial role in stopping power at low velocities [40] because they belong to the first shell of bound electrons below the conduction band. As was pointed out [41], the extraordinarily high stopping cross section observed for protons in Gd and Ta cannot be understood in terms of the FEG model, which casts doubt on its accurate description for  $S_e$ . Nonrelativistic calculation is inadequate for the description of the electronic structure of heavy targets. Relativistic effects are required to be taken into account for elements with atomic number  $Z > 54$  [42]. The influence of relativistic corrections on electronic structure and electronic stopping is an important research focus in heavy targets [42–45].

Given the recent interest in this class of materials, this paper focuses on the  $S_e$  of protons in Pt and discusses the physical mechanism of the stopping process that occurs in the femtosecond timescale, with an explicit simulation of electron dynamics. In this paper, we study the channeling and off-channeling  $S_e$  of Pt for protons. Whether  $f$ -electron excitation causes the  $S_e$  to deviate from the velocity proportionality in the low-energy region, and the contribution of  $f$ -electron excitation to the  $S_e$  are studied in a wide velocity range. The relativistic effect of the host electrons on the  $S_e$  of Pt is clarified. In addition, the mean steady-state charge of protons interacting with Pt is analyzed. Our aim is not only to improve the compilation [43] of stopping power data, but also to provide insight into the underlying physics of protons interacting with Pt.

## II. METHOD AND COMPUTATIONAL DETAILS

The electronic stopping of protons traversing Pt is simulated by Ehrenfest molecular dynamics combined with the time-dependent density functional theory (EMD-TDDFT) model [46–48]. The combined application of time-dependent density functional theory calculations for electrons and molecular dynamics simulations for ions makes it possible to study the nonequilibrium response of the electronic subsystem of the target to ions irradiation and to calculate the nonadiabatic energy exchange between the energetic ions and the host electrons [49]. The time-dependent Kohn-Sham (TDKS) equations describing the single-particle wave function  $\varphi_i$  of individual electrons are (in atomic units)

$$i \frac{\partial \varphi_i(\mathbf{r}, t)}{\partial t} = \left[ -\frac{1}{2} \nabla^2 + V_{\text{KS}}[n, \{\mathbf{R}_J(t)\}](\mathbf{r}, t) \right] \varphi_i(\mathbf{r}, t), \quad (1)$$

where  $\mathbf{R}_J(t)$  is the time-dependent coordinate of the  $J$ th nucleus. The Kohn-Sham effective potential  $V_{\text{KS}}(\mathbf{r}, t)$  is conceptually partitioned in three contributions:

$$V_{\text{KS}}[n, \{\mathbf{R}_J\}](\mathbf{r}, t) = V_{\text{ext}}[\{\mathbf{R}_J\}](\mathbf{r}, t) + V_{\text{H}}[n](\mathbf{r}, t) + V_{\text{XC}}[n](\mathbf{r}, t), \quad (2)$$

in which  $V_{\text{ext}}(\mathbf{r}, t)$  is the time-dependent electron-nucleus potential,  $V_{\text{H}}[n](\mathbf{r}, t)$  is the Hartree potential which describes the classical electrostatic interaction between electrons, and  $V_{\text{XC}}[n](\mathbf{r}, t)$  presents the time-dependent exchange-correlation potential. The adiabatic local density approximation (ALDA) with Perdew-Wang parametrization [50] for the exchange-correlation (XC) potential is employed in the time-evolving calculations. The electron density of the system is given by

$$n(\mathbf{r}, t) = 2 \sum_i |\varphi_i(\mathbf{r}, t)|^2. \quad (3)$$

A  $2 \times 2 \times 3$  face-centered cubic supercell consisting of 48 Pt atoms is employed to model bulk Pt. Periodic boundary conditions are used throughout this study. Ewald summation [51,52] is employed to sum the long-range interactions between ions in periodic images. The interaction between electrons and ionic cores is described by the norm-conserving Troullier-Martins pseudopotential [53]. To clarify the contribution of  $f$ -electron excitation on the electronic energy loss of protons, we constructed two pseudopotential models with 10

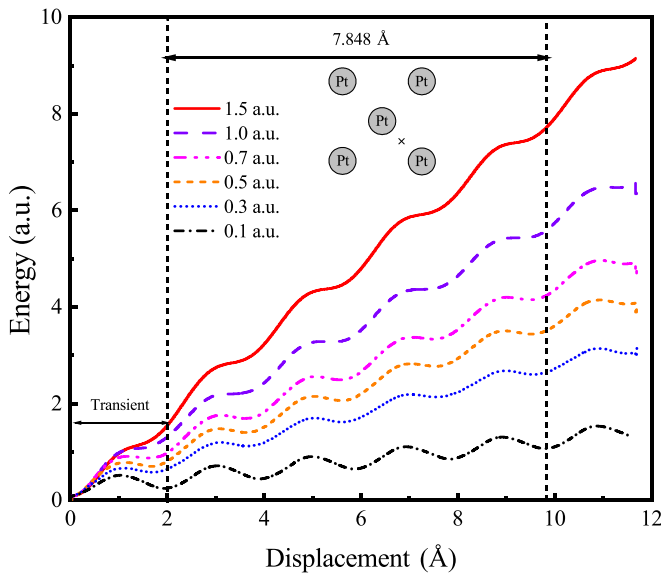


FIG. 1. Total energy increment as a function of proton displacement in the  $\langle 001 \rangle$  trajectory at various velocities. The region on the left side of the first vertical dotted line denotes the transient phase. The inset shows the top view of the incidence geometry. The gray circles represent the platinum atoms and the black fork indicates the impact location of the protons.

and 24 valence electrons for the Pt atom, which are labeled as Pt10 ( $[\text{Xe}4f^{14}]5d^96s^1$ ) and Pt24 ( $[\text{Xe}]4f^{14}5d^96s^1$ ) in the present study, respectively. To assess the importance of the relativistic effect of the bound and the valence electrons, a fully relativistic pseudopotential model for Pt atom was also developed, denoted as “Pt24-rel”. The wave functions, electron densities, and external potentials are discretized in a real space grid with uniform spacing of 0.14 Å along all three spatial coordinates in the simulation cell.

In this theoretical framework, the ground-state Kohn-Sham orbitals of Pt are achieved by diagonalization of the time-independent Kohn-Sham Hamiltonian. The time-dependent evolution of energy can be obtained by solving the TDKS equations. In the real time evolution, the host atoms are held fixed at their equilibrium positions, the protons are given an initial velocity and constrained to move along both channeling and off-channeling trajectories, respectively. Fixing the host atoms in their equilibrium positions ensures that the ion energy is transferred only to the electronic subsystem of Pt through inelastic collisions. We set different propagation step length so that  $\Delta t \times v \sim 2.59 \times 10^{-3}$  Å for various velocities, which is used to ensure the convergence of the total energy. The methods described here, including approximations for the electron interactions, display that a good balance between computational accuracy and efficiency is achieved when dealing with solid systems [38,54,55].

In this work, the protons are traveling along the  $\langle 001 \rangle$  crystal axis of Pt in the channeling geometry and the incident point for the channeling trajectory is shown in the inset of Fig. 1. Figure 1 shows the total energy increment of Pt supercell as a function of the proton displacement in the channeling geometry. The electronic subsystem of Pt is in the ground state prior to the time-dependent evolution, which increases

as the protons are forced to move at a constant velocity  $v$ . The protons produce electronic excitations, a nonadiabatic behavior that increases the electronic energy. The energy of protons is gradually deposited into the electronic subsystem of Pt and the total energy growth rate of the projectile-target system is equal to that of the electronic subsystem of Pt (in the experiments, this happens at the expense of the ion kinetic energy; in the simulation, the ion kinetic energy is held constant for simplicity). The instantaneous  $S_e$  is identified as the total energy  $E(x)$  growth rate with respect to proton displacement  $x$ ,  $S_e = dE(x)/dx$ . As shown in the figure, the protons reach an equilibrium charge state rapidly when the projectiles begin to move in Pt, marked by a vertical dashed line on the left side. A “transient” of the electronic energy is caused by the sudden movement of ions and the charge exchange between the projectiles and the host atoms, which is prominent in the low-energy region [38,54]. To avoid the effect of the “transient” on the  $S_e$ , we extracted the instantaneous  $S_e$  after the ions reach the equilibrium charged state [38]. The growth of the total energy shows the smooth oscillations in the region in which the equilibrium charge state is achieved, which is correlated with the lattice periodicity of Pt. The equilibrium  $S_e$  is obtained by averaging the instantaneous  $S_e$  over two lattice periods between the two vertical dashed lines as indicated in Fig. 1.

To be more consistent with the projectiles traveling in random directions in the host material (i.e., the off-channeling case) as in most experiments, the protons not only travel in a specific direction, but also in disordered directions through the lattice in our simulations. The protons accidentally enter the core region of the host atoms in the off-channeling geometry, causing the core electrons’ excitation. A practical method to calculate the off-channeling stopping is to average the  $S_e$  obtained from many off-channeling trajectories. Here, four incident directions [0.309, 0.500, 0.809], [0.304, 0.952], [0.320, 0.893, 0.317], and [0.444, 0.513, 0.735] are selected following Ref. [54] (given as normalized here), and three impact parameters were selected for each direction to obtain 12 off-channeling trajectories, the off-channeling stopping is obtained by averaging the  $S_e$  of the 12 trajectories at each velocity. Notably, these incident directions are selected to avoid the head-to-head collision between ions and host atoms. In addition, the finite-size effects were studied for a larger supercell ( $3 \times 3 \times 3$ ) including 108 Pt atoms, for selected velocities with negligible difference within 1.0%. The calculations are performed by using the OCTOPUS code [56,57].

### III. RESULTS AND DISCUSSION

Figure 2(a) shows the electron binding energy of the Pt atom obtained from theoretical calculations with or without relativistic correction, along with the experimental data for solid Pt [58]. Experimental results only give the electron binding energy of the  $1s$  to  $4f$  shell, while we also calculate the binding energy of  $5d$  and  $6s$  electrons. The figure clearly shows that nonrelativistic calculations cannot accurately describe the experimental binding energies of the inner shells, but the overall agreement between the present relativistic binding energies and the experimental data is very good. The nonrelativistic binding energies underestimate the

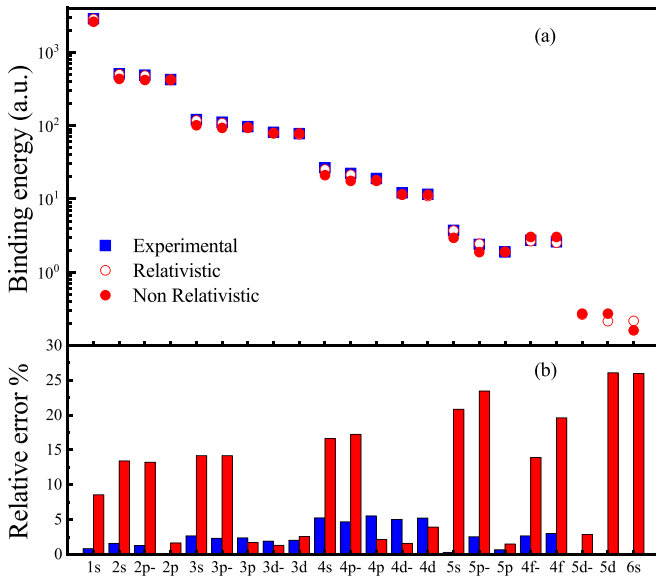


FIG. 2. (a) Binding energies of Pt. Relativistic and nonrelativistic results are represented by empty and solid circles respectively, and experimental measurements for solid Pt [58] are represented by squares. (b) Corresponding relative errors with respect to relativistic results.

experimental data except for the  $4f$  shell. The electron binding energy of the  $6s$  shell becomes larger as the relativistic correction is considered, while it becomes smaller for the  $5d$  and  $4f$  shells. More details about the binding energies are given in Fig. 2(b). The blue and red bars represent the relative errors of the experimental and nonrelativistic binding energies with respect to the relativistic results, respectively. The relativistic binding energy agrees with experimental data within 5% for  $1s$  to  $4f$  shells. The relative errors of the nonrelativistic binding energy with respect to the relativistic results for  $4f$  and valence electron shells are 20% and 25%, respectively. The results show that the relativistic effect poses a significant influence on  $5d$  and  $6s$  electrons in comparison with  $4f$  electrons; this is because the  $4f$  electrons are spatially localized compared to  $5d$  and  $6s$  electrons.

The  $S_e$  of Pt for protons moving along the channeling and the off-channeling trajectories obtained from RT-TDDFT calculation is shown in Fig. 3, as well as the experimental data [59,60]. Also shown are the DFT calculation based FEG predictions [61] with the Wigner-Seitz radius  $r_s = 2.30$  a.u. and  $r_s = 1.34$  a.u., which corresponds to two and ten electrons per Pt atom, respectively. As expected, the  $S_e$  for protons traveling along the channeling and off-channeling trajectories from the three pseudopotential models do not deviate from velocity proportionality in the low velocity range. In Fig. 3(a), the channeling  $S_e$  including  $5d$  and  $6s$  electrons as well as the FEG prediction with  $r_s = 2.30$  a.u. significantly underestimates the experimental data. The channeling  $S_e$  obtained from Pt24 and Pt24-rel pseudopotential models displays a significant improvement and is in agreement with the experimental data and FEG prediction with  $r_s = 1.34$  a.u. Compared with the channeling  $S_e$  calculated from the Pt10 model, the  $S_e$  obtained from Pt24 and Pt24-rel models showed that the  $4f$  electrons are excited in the low velocity range. The channeling stopping

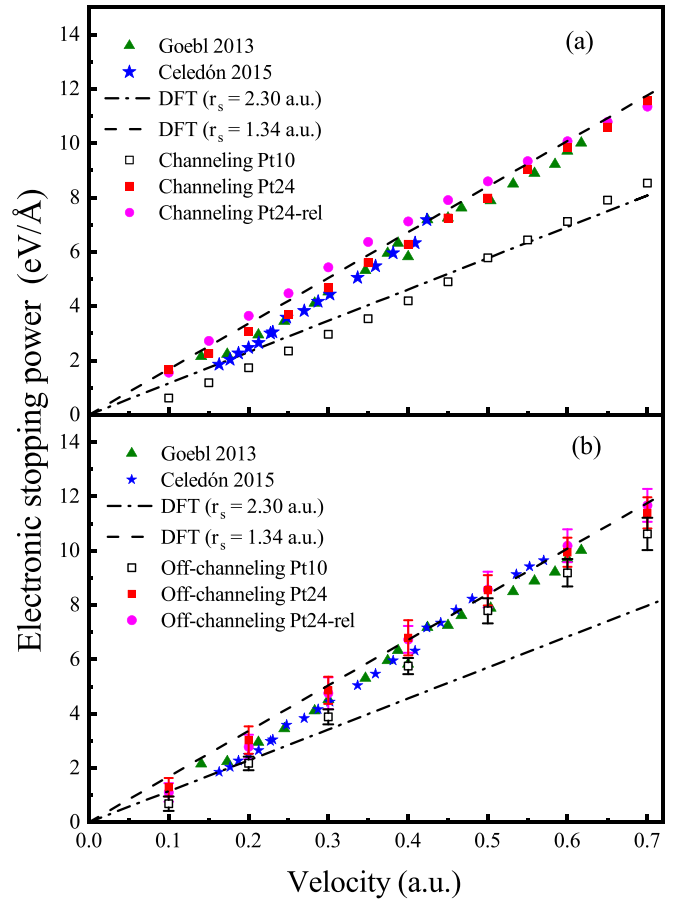


FIG. 3. Electronic stopping power obtained from RT-TDDFT calculations are shown as a function of velocity for protons moving along (a) the channeling and (b) off-channeling trajectories in Pt. Experimental data are from Refs. [59,60]. FEG predictions [61] with Wigner-Seitz radius  $r_s = 1.34$  a.u. and  $r_s = 2.30$  a.u. based on DFT calculation are also displayed.

is slightly increased from 0.15 to 0.60 a.u. considering the relativistic correction.

In Fig. 3(b), the off-channeling  $S_e$  obtained from Pt10 pseudopotential model underestimates the FEG predictions with  $r_s = 1.34$  a.u. in the low-energy range. The off-channeling  $S_e$  from Pt24 and Pt24-rel pseudopotential models is slightly higher than that from the Pt10 pseudopotential. The agreement between the  $S_e$  including also the  $f$ -electron excitation and the FEG predictions with  $r_s = 1.34$  a.u. is very good at  $v > 0.40$  a.u. It can be seen clearly that, the FEG predictions with  $r_s = 2.30$  a.u. significantly underestimate the experimental data and the RT-TDDFT calculation results at  $v > 0.20$  a.u. The improvement on the off-channeling  $S_e$  from the Pt10 pseudopotential is mainly due to the contribution of  $5d$ -electron excitation. It can be seen from Fig. 3(b) that the  $d$ -electron excitation is dominant at  $v > 0.20$  a.u., so the FEG predictions with  $r_s = 2.30$  a.u. is not sufficient to describe the  $S_e$ . The off-channeling  $S_e$  of Pt is not affected by the relativistic correction in the low-energy region. Our RT-TDDFT off-channeling stopping obtained from Pt10, Pt24, and Pt24-rel pseudopotentials is in good agreement with the experimental data, indicating that the valence electrons



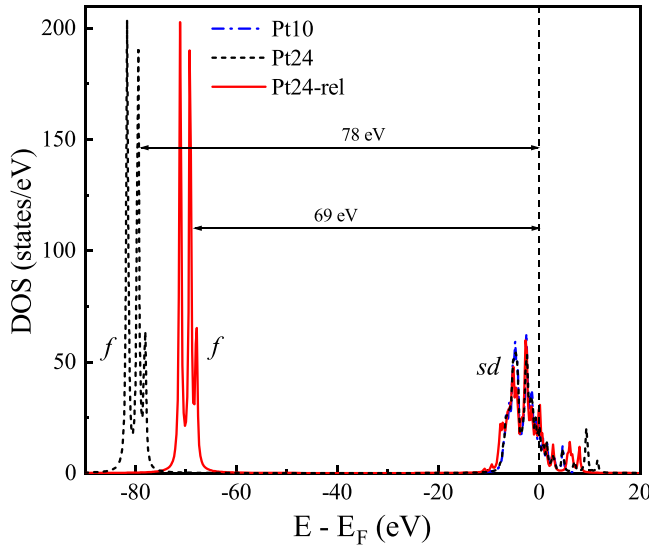


FIG. 4. Electronic DOS of Pt is shown as function of  $E-E_F$ . The dash-dotted, short-dashed, and solid lines represent the results obtained from Pt10, Pt24, and Pt24-rel pseudopotential models, respectively.  $E_F$  represents the Fermi energy of Pt.

( $5d^96s^1$ ) are sufficient to describe the off-channeling  $S_e$  of Pt in the low-velocity regime.

The electronic density of states (DOS) of Pt is shown in Fig. 4. As shown in Fig. 4, the energy of  $5d$ -electron band has been extended to the Fermi energy of Pt. At very low projectile velocities, the energy loss is due to the excitation of electrons with energies close to the Fermi level. Therefore, our RT-TDDFT calculations show that the  $S_e$  considering  $5d$  and  $6s$  electrons is proportional to the ion velocity, which is consistent with the experimental results [32,41,60]. With increasing ion energies, more electrons are incorporated to the energy loss and the stopping power gradually approaches the velocity proportionality predicted by the FEG model including more inner shell electrons. The threshold velocity for excitation of  $f$ -electron to the Fermi level can be calculated by the following equation:

$$v_{\text{th}} = \frac{E_f}{2\hbar k_F}, \quad (4)$$

where  $E_f$  represents the  $f$ -band offset, which is the energy interval between the edge of the  $f$ -band and the Fermi energy level of Pt. The  $f$  states for Pt24 and Pt24-rel models are located at  $\sim 78$  and  $69$  eV below  $E_F$ , i.e., the  $E_f = 78$  and  $69$  eV, respectively. The Fermi wave vector  $k_F = 1.92/r_s = 1.43/a_0$  is for the effective uniform electron gas containing  $5d$  and  $6s$  electrons of Pt ( $r_s = 1.34$  a.u.). According to Eq. (4), the calculated threshold velocity  $v_{\text{th}} = 1.00$  a.u. and  $0.89$  a.u. for Pt24 and Pt24-rel models, respectively. Therefore, the static DFT prediction shows that the valence electron ( $5d$  and  $6s$ ) excitation plays a dominant role in the low-energy  $S_e$ , while the inner  $f$  electrons do not get excited in the low-energy region. However, The RT-TDDFT results show that the  $f$ -electron is excited in the low-energy region. The threshold effect for the  $f$ -electron excitation is not displayed by the RT-TDDFT calculations, suggesting that the participation of core electrons

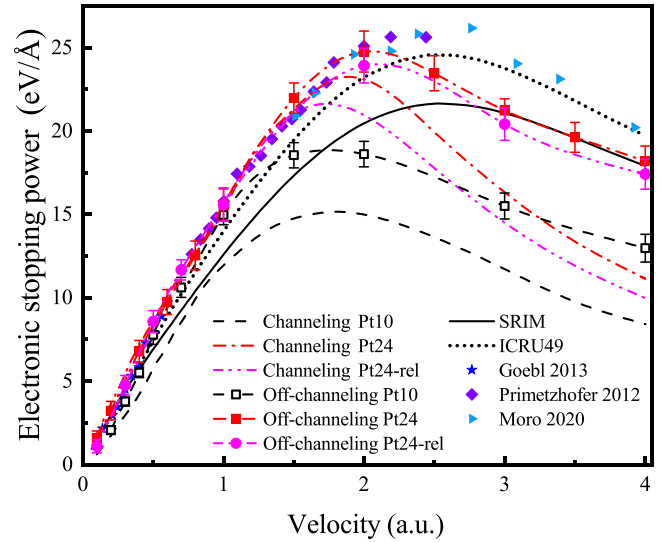


FIG. 5. Electronic stopping power of Pt for protons moving along channeling geometry and off-channeling geometry and compared with experimental measurements [32,40,59]. The solid line is the stopping power predicted by the SRIM-2013 package. The dotted line represents the  $S_e$  given by ICRU49 database [62].

excitation is not a sufficient condition for the appearance of the threshold effect.

The  $S_e$  of Pt for protons is extended to 4.0 a.u., and the results are shown in Fig. 5. We compare the channeling stopping of protons traveling along the (001) axis and the off-channeling stopping with the SRIM database, ICRU49 database [62], and the experimental data [32,40,59]. The ICRU49 report contains the stopping power and range tables for protons and alpha particles, and the tabulated stopping power is based on experimental data at the low-energy region; the stopping power is based on Bethe's stopping power theory with semi-empirical mean excitation energies and shell corrections at the high-energy region, and with corrections for departures from the first Born approximation. As a result, the  $S_e$  obtained from ICRU49 is greatly improved compared to the SRIM data, approaching the experimental data. For the channeling geometry, the  $S_e$  including only valence electrons ( $5d$  and  $6s$  electrons) is lower than the ICRU49 results and the experimental data by 59.29% at  $v = 4.0$  a.u. The  $S_e$  including also  $f$ -electron excitation is increased by 32.35%, and the  $S_e$  including also  $f$ -electron excitation with relativistic correction is increased by 18.53% at  $v = 4.0$  a.u. Even after including the  $f$ -electron excitation contribution, the channeling  $S_e$  significantly underestimates the experimental data beyond the stopping maximum. The  $S_e$  obtained from Pt24 and Pt24-rel pseudopotential models agrees well with the experimental data up to 1.5 a.u., while it underestimates the experimental data and ICRU49 predictions towards higher velocities. The excitation energy of  $4f$  electrons decreases by considering the relativistic correction, resulting in a lower  $S_e$  obtained from Pt24-rel than that from Pt24 in the high-energy region.

Considering the higher excitation efficiency of inner electrons in the off-channeling geometry, the off-channeling  $S_e$  including also  $4f$  electrons is calculated. The off-channeling  $S_e$  containing only valence electrons is in good agreement

with the ICRU49 predictions and experimental data up to 1.0 a.u. The off-channeling  $S_e$ , including also the 4*f* electron excitation, agrees well with the experimental data until the stopping maximum. It can be seen that the off-channeling  $S_e$  obtained from Pt24 and Pt24-rel pseudopotential models deviates from that obtained from the Pt10 model towards higher values at  $v > 1.0$  a.u., and this deviation becomes considerable at higher velocities, which is in line with the DOS distribution of the *f* states of Pt. This is consistent with the fact that the excitation of the *f*-electron is possible already at very low velocities and becomes considerable at higher velocities [41]. The results show that the contribution of 4*f* electrons to  $S_e$  is beyond doubt in the high-energy region. Compared with the channeling stopping, the off-channeling  $S_e$  is significantly improved in the high-energy region, approaching the experimental data. The off-channeling  $S_e$  containing 5*d* and 6*s* electrons is lower by 34.19% in comparison with the experimental data at  $v = 4.0$  a.u. The  $S_e$  obtained from Pt24 and Pt24-rel models is lower than the experimental data by 7.56% and 11.67%, respectively. The off-channeling  $S_e$  with *f*-electron excitation is consistent with SRIM results at  $v > 3.0$  a.u. Furthermore, we noticed that the maximum of  $S_e$  containing only 5*d* and 6*s* excitation is located at 1.75 a.u., while the maximum of  $S_e$  including also *f*-electron excitation is displaced at 2.0 a.u. Thus, the participation of the *f*-electron in the electronic stopping dynamics moves the stopping maximum position towards a higher energy.

To understand the contribution of conduction and bound electrons excitation to  $S_e$ , the time-dependent occupation number of the Kohn-Sham states of Pt in the nonadiabatic simulations can be calculated by projecting the time-dependent Kohn-Sham wave function  $|\psi_{n'}(t)\rangle$  onto the ground-state wave function  $|\phi_n\rangle$ . The number of excited electrons  $n_{\text{ex}}$  can be obtained by the following formula [63]:

$$n_{\text{ex}}(t) = \sum_{nm'}^{n_{\text{occ}}} f_n [1 - |\langle \phi_n | \psi_{n'}(t) \rangle|^2], \quad (5)$$

$n_{\text{occ}}$  is the number of occupied states,  $f_n$  is the fixed occupation of the Kohn-Sham state  $|\phi_n\rangle$  ( $f = 2$  for occupied states). We obtained the number of excited electrons from Pt24 and Pt24-rel models for protons traveling along the channeling trajectory, and then calculated the ratio of electrons excited from each band of Pt to the total number of excited electrons as a function of proton velocity, as shown in Fig. 6. It can be seen that the discrepancy in the ratio of electrons excited from each band in Pt24 and Pt24-rel pseudopotential models is due to the relativistic correction. The ratio of electrons excited from the 4*f* band is almost the same in both pseudopotential models at  $v \leq 2.5$  a.u., while the ratio for Pt24-rel model is slightly higher than that for Pt24 model beyond this velocity region. The results show that the contribution of *f*-electron excitation to  $S_e$  is significant in the high-energy region, accounting for about 14.0% of the total electronic excitations. The contribution of 5*d* and 6*s* electronic excitations to the total excitations is 86.0%, respectively. The results show that the 5*d* electrons are excited at very low velocity, so the threshold effect for 5*d*-electron excitation does not appear. The contribution of 5*d*-electron excitation to the  $S_e$  is significant.

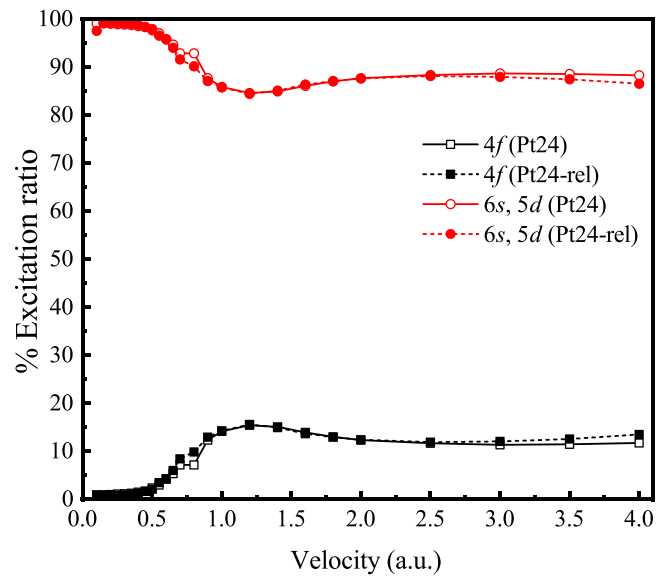


FIG. 6. The ratio of electrons excited from 4*f* band, 5*d* and 6*s* bands relative to the total number of excited electrons, respectively. Empty and solid symbols indicate results obtained from Pt24 and Pt24-rel models, respectively.

The advantage of using the RT-TDDFT method is that it provides insight into the charges of the projectiles traveling through the host materials and it can be compared with validated models [64–66]. The challenge is that the charge (or degree of ionization) of the ions is not well defined in the theoretical framework and a sensible determination method is relied on separating the charges captured by the ions from the host electrons. A reasonable partitioning scheme is employed to quantify the nonequilibrium electron density border between the ions and the host atoms in our RT-TDDFT simulations. The charges captured by the protons are considered to be distributed in a sphere, and the proton position is the center of the sphere. The lowest electron density between the ions and the host atoms is considered to be the border for the electron density. The distance from the center of the sphere to the border is regarded as the distribution radius for the effective charge of ions. The determination of the effective charge radius follows that of the authors of Ref. [67]. Using this method, the effective charge radius for protons is determined for each ion velocity and the charges captured by the protons are obtained by integrating the electron density within the spheres.

In Fig. 7, we present the instantaneous charge state as a function of the proton displacement for  $v = 0.1$  a.u., 0.5 a.u., 1.0 a.u., 1.5 a.u., 2.0 a.u., and 3.0 a.u., respectively. The instantaneous charge state of the projectiles is obtained by subtracting the captured charges from the initial charge state of bare protons. The protons capture charges as they approach the host atoms and lose charges as they go away from the host atoms, resulting in the oscillation of the instantaneous charge state of the protons. That the oscillation of the instantaneous charge state of the protons with respect to the displacement reflects the periodicity of the lattice structure of Pt. This is a cyclic dynamic process in the trajectory of ion movement. Therefore, the alternate neutralization and

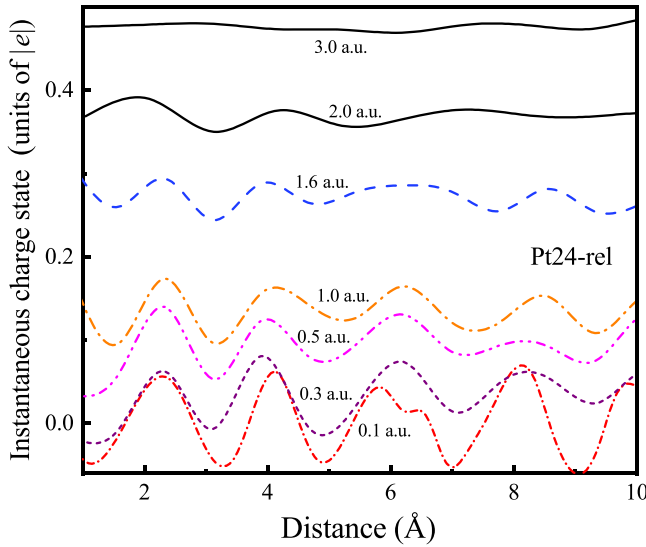


FIG. 7. The instantaneous charge state of protons as a function of displacement in the (001) channel. The results are obtained from the Pt24-rel pseudopotential.

re-ionization processes were displayed for the protons traveling in the channeling condition. The periodic oscillations at some velocities can be seen in Fig. 7, while the instantaneous charge of ions does not change periodically beyond the stopping maximum velocity. This is true at 3.0 a.u., for example, because the protons capture less charges at higher velocities.

The mean steady-state charge ( $\bar{q}$ ) of channeling protons as a function of velocity is shown in Fig. 8. To rule out the influence of electron density of the host atoms on the determination of the charge state of ions, the charge state of protons is counted in interstitial sites where the target electron density is the lowest. This is an analysis method based

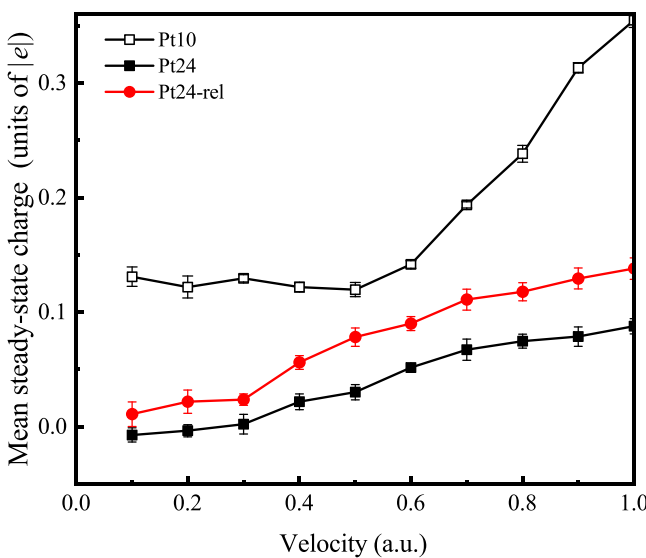


FIG. 8. The mean steady-state charge as a function of proton velocity. Solid and empty squares indicate the results with  $4f$  electron considered or not, respectively. The circles represent the results with relativistic effect.

on electron density and cannot be regarded as an accurate description of the charge transfer due to the locality nature of the time-dependent adiabatic local density approximation (TD-ALDA) [68]. This is why the protons capture more than one electron at very low velocities. In addition, the quantitative analysis of the charge state of projectiles is also affected by the assumption that the electron density of projectiles is spherically distributed. It can be seen from Fig. 8 that the mean steady-state charge of protons obtained from the Pt10 pseudopotential is always higher than those obtained from Pt24 and Pt24-rel pseudopotentials, which suggests that the charge state of protons is lowered by the participation of inner electron excitation [69]. The mean steady-state charge of protons in the Pt24-rel pseudopotential is higher than that in the Pt24 pseudopotential. This is the reason why the  $S_e$  obtained by the Pt24-rel pseudopotential is higher than that obtained by the Pt24 pseudopotential for velocities below 0.6 a.u., as shown in Fig. 3(a).

#### IV. CONCLUSION

In summary, we present a first-principles calculation of the  $S_e$  of protons traveling through Pt in both channeling and off-channeling geometries based on RT-TDDFT electron dynamics. Our results show that the  $f$ -electron is excited in the low-energy region and the channeling and off-channeling  $S_e$ , including also the  $f$ -electron, do not deviate from the velocity proportionality. In the off-channeling case, our RT-TDDFT calculation is in agreement with the experimental data and the excitation efficiency of  $5d$  electrons is greatly improved. The valence electron excitation is sufficient to accurately describe the  $S_e$  of Pt in the low-energy region. In the intermediate energy region, our results display that the stopping maximum position moves towards to higher energy due to the participation of the  $f$ -electron in the electron stopping dynamics. In the high-energy region, the channeling  $S_e$  containing also  $f$ -electron excitation agrees with the experimental data up to 1.5 a.u. Compared with the channeling  $S_e$ , the off-channeling results improves  $S_e$  significantly and it is in a good agreement with the experimental data up to the stopping maximum. The excitation of the  $f$ -electron contributes to about 14.0% of the total electronic excitations in the high-energy range. In addition, the instantaneous charge state and the mean steady-state charge of protons are analyzed. The results showed that the instantaneous charge states of low-energy protons exhibit periodic oscillations, and charge transfer is a very important energy loss channel in the low-energy region.

#### ACKNOWLEDGMENTS

This work was supported by the National Natural Science Foundation of China under Grants No. 11975119, No. 11774030, and No. 12135004. B.-S.L. acknowledges Sichuan Science and Technology Program (Grant No. 2020ZYD055) for financial support.

- [1] S. N. Markin, D. Primetzhofer, M. Spitz, and P. Bauer, *Phys. Rev. B* **80**, 205105 (2009).
- [2] F. Aumayr, S. Facsko, A. S. El-Said, C. Trautmann, and M. Schlegelberger, *J. Phys.: Condens. Matter* **23**, 393001 (2011).
- [3] Z. Li and F. Chen, *Appl. Phys. Rev.* **4**, 011103 (2017).
- [4] G. S. Was, *Fundamentals of Radiation Material Science: Metals and Alloys*, 1st ed., (Springer, New York, 2007).
- [5] J. W. Mayer and E. Rimini, *Ion Beam Handbook for Material Analysis* (Academic, Cambridge, MA, 1977).
- [6] P. D. Townsend, P. J. Chandler, and L. Zhang, *Optical Effects of Ion Implantation* (Cambridge University Press, Cambridge, England, 1994).
- [7] S. Duzellier, *Aerosp. Sci. Technol.* **9**, 93 (2005).
- [8] J. Sisterson, *Nucl. Instrum. Methods Phys. Res. Sect. B* **241**, 713 (2005).
- [9] J. S. Loeffler and M. Durante, *Nat. Rev. Clin. Oncol.* **10**, 411 (2013).
- [10] M. T. Robinson and I. M. Torrens, *Phys. Rev. B* **9**, 5008 (1974).
- [11] K. Arstila, J. Keinonen, P. Tikkanen, and A. Kuronen, *Phys. Rev. B* **43**, 13967 (1991).
- [12] A. Valenzuela, W. Meckbach, A. J. Kestelman, and J. C. Eckardt, *Phys. Rev. B* **6**, 95 (1972).
- [13] A. Lurio, J. F. Ziegler, and J. J. Cuomo, *Nucl. Instrum. Methods* **149**, 155 (1978).
- [14] D. A. Thompson, W. F. S. Poehlman, P. Presunka, and J. A. Davies, *Nucl. Instrum. Methods Phys. Res.* **191**, 469 (1981).
- [15] P. Bauer, *Nucl. Instrum. Methods Phys. Res. Sect. B* **45**, 673 (1990).
- [16] J. J. Dorado and F. Flores, *Phys. Rev. A* **47**, 3062 (1993).
- [17] I. Abril, R. Garcia-Molina, C. D. Denton, F. J. Pérez-Pérez, and N. R. Arista, *Phys. Rev. A* **58**, 357 (1998).
- [18] J. I. Juaristi, C. Auth, H. Winter, A. Arnau, K. Eder, D. Semrad, F. Aumayr, P. Bauer, and P. M. Echenique, *Phys. Rev. Lett.* **84**, 2124 (2000).
- [19] N. R. Arista, *Nucl. Instrum. Methods Phys. Res. Sect. B* **195**, 91 (2002).
- [20] J. Sillanpää, E. Vainonen-Ahlgren, P. Haussalo, and J. Keinonen, *Nucl. Instrum. Methods Phys. Res., Sect. B* **142**, 1 (1998).
- [21] C. C. Montanari and J. E. Miraglia, *Phys. Rev. A* **96**, 012707 (2017).
- [22] E. Fermi and E. Teller, *Phys. Rev.* **72**, 399 (1947).
- [23] G. Martínez-Tamayo, J. C. Eckardt, G. H. Lantschner, and N. R. Arista, *Phys. Rev. A* **54**, 3131 (1996).
- [24] H. Bitao, L. Zhaoyuan, and Q. Zhong, *Nucl. Instrum. Methods Phys. Res., Sect. B* **149**, 395 (1999).
- [25] S. P. Møller, A. Csete, T. Ichioka, H. Knudsen, U. I. Uggerhøj, and H. H. Andersen, *Phys. Rev. Lett.* **93**, 042502 (2004).
- [26] C. Celedón, E. A. Sánchez, M. S. Moreno, N. R. Arista, J. D. Uribe, M. Mery, J. E. Valdés, and P. Vargas, *Phys. Rev. A* **88**, 012903 (2013).
- [27] J. E. Valdés, J. C. Eckardt, G. H. Lantschner, and N. R. Arista, *Phys. Rev. A* **49**, 1083 (1994).
- [28] E. Runge and E. K. U. Gross, *Phys. Rev. Lett.* **52**, 997 (1984).
- [29] E. D. Cantero, G. H. Lantschner, J. C. Eckardt, and N. R. Arista, *Phys. Rev. A* **80**, 032904 (2009).
- [30] S. N. Markin, D. Primetzhofer, S. Prusa, M. Brunmayr, G. Kowarik, F. Aumayr, and P. Bauer, *Phys. Rev. B* **78**, 195122 (2008).
- [31] M. A. Zeb, J. Kohanoff, D. Sánchez-Portal, A. Arnau, J. I. Juaristi, and E. Artacho, *Phys. Rev. Lett.* **108**, 225504 (2012).
- [32] D. Primetzhofer, *Phys. Rev. B* **86**, 094102 (2012).
- [33] R. A. Wilhelm, E. Gruber, R. Ritter, R. Heller, S. Facsko, and F. Aumayr, *Phys. Rev. Lett.* **112**, 153201 (2014).
- [34] D. C. Yost and Y. Kanai, *Phys. Rev. B* **94**, 115107 (2016).
- [35] K. G. Reeves, Y. Yao, and Y. Kanai, *Phys. Rev. B* **94**, 041108(R) (2016).
- [36] J. F. Ziegler, M. Ziegler, and J. Biersack, *Nucl. Instrum. Methods Phys. Res., Sect. B* **268**, 1818 (2010).
- [37] A. Ojanperä, A. V. Krasheninnikov, and M. Puska, *Phys. Rev. B* **89**, 035120 (2014).
- [38] A. Schleife, Y. Kanai, and A. A. Correa, *Phys. Rev. B* **91**, 014306 (2015).
- [39] E. E. Quashie and A. A. Correa, *Phys. Rev. B* **98**, 235122 (2018).
- [40] M. V. Moro, P. Bauer, and D. Primetzhofer, *Phys. Rev. A* **102**, 022808 (2020).
- [41] D. Roth, B. Bruckner, M. V. Moro, S. Gruber, D. Goebel, J. I. Juaristi, M. Alducin, R. Steinberger, J. Duchoslav, D. Primetzhofer, and P. Bauer, *Phys. Rev. Lett.* **118**, 103401 (2017).
- [42] C. C. Montanari, C. D. Archubi, D. M. Mitnik, and J. E. Miraglia, *Phys. Rev. A* **79**, 032903 (2009).
- [43] C. C. Montanari, D. M. Mitnik, C. D. Archubi, and J. E. Miraglia, *Phys. Rev. A* **80**, 012901 (2009).
- [44] E. Engel, R. M. Dreizler, S. Varga, and B. Fricke, *Relativistic Effects in Heavy-Element Chemistry and Physics*, edited by B. A. Hess, (John Wiley and Sons, New York, 2001).
- [45] C. C. Montanari, P. A. Miranda, E. Alves, A. M. P. Mendez, D. M. Mitnik, J. E. Miraglia, R. Correa, J. Wachter, M. Aguilera, N. Catarino, and R. C. da Silva, *Phys. Rev. A* **101**, 062701 (2020).
- [46] X. Andrade, A. Castro, D. Zueco, J. L. Alonso, P. Echenique, F. Falseto, and A. Rubio, *J. Chem. Theory Comput.* **5**, 728 (2009).
- [47] J. L. Alonso, X. Andrade, P. Echenique, F. Falseto, D. Prada-Gracia, and A. Rubio, *Phys. Rev. Lett.* **101**, 096403 (2008).
- [48] A. Castro, M. Isla, J. I. Martínez, and J. A. Alonso, *Chem. Phys.* **399**, 130 (2012).
- [49] M. A. Zeb, J. Kohanoff, D. Sánchez-Portal, and E. Artacho, *Nucl. Instrum. Methods Phys. Res., Sect. B* **303**, 59 (2013).
- [50] J. P. Perdew and Y. Wang, *Phys. Rev. B* **45**, 13244 (1992).
- [51] H. D. Hecce, A. E. Garcia, and T. Darden, *J. Chem. Phys.* **126**, 124106 (2007).
- [52] B. A. Wells and A. L. Chaffee, *J. Chem. Theory Comput.* **11**, 3684 (2015).
- [53] N. Troullier and J. L. Martins, *Phys. Rev. B* **43**, 1993 (1991).
- [54] E. E. Quashie, B. C. Saha, and A. A. Correa, *Phys. Rev. B* **94**, 155403 (2016).
- [55] E. E. Quashie, X. Andrade, and A. A. Correa, *Eur. Phys. J. D* **75**, 280 (2021).
- [56] X. Andrade, D. A. Strubbe, U. De Giovannini, A. H. Larsen, M. J. T. Oliveira, J. Alberdi-Rodriguez, A. Varas, I. Theophilou, N. Helbig, M. Verstraete, L. Stella, F. Nogueira, A. Aspuru-Guzik, A. Castro, M. A. L. Marques, and A. Rubio, *Phys. Chem. Chem. Phys.* **17**, 31371 (2015).
- [57] X. Andrade, J. Alberdi-Rodriguez, D. A. Strubbe, M. J. T. Oliveira, F. Nogueira, A. Castro, J. Muguerza, A. Arruabarrena, S. G. Louie, A. Aspuru-Guzik, A. Rubio, and M. A. L. Marques, *J. Phys.: Condens. Matter* **24**, 233202 (2012).



- [58] G. P. Williams, *Electron Binding Energies of the Elements*, available from [http://xdb.lbl.gov/Section1/Sec\\_1-1.html](http://xdb.lbl.gov/Section1/Sec_1-1.html).
- [59] D. Goebel, D. Roth, and P. Bauer, *Phys. Rev. A* **87**, 062903 (2013).
- [60] C. E. Celedón, E. A. Sánchez, L. Salazar Alarcón, J. Guimpel, A. Cortés, P. Vargas, and N. R. Arista, *Nucl. Instrum. Methods Phys. Res., Sect. B* **360**, 103 (2015).
- [61] J. I. Juaristi, M. Alducin, R. Díez Muiño, H. F. Busnengo, and A. Salin, *Phys. Rev. Lett.* **100**, 116102 (2008).
- [62] ICRU report 49, Stopping Powers and Ranges for Protons and Alpha Particles, International Commission on Radiation Units and Measurements, 1993.
- [63] T. Otobe, M. Yamagiwa, J. I. Iwata, K. Yabana, T. Nakatsukasa, and G. F. Bertsch, *Phys. Rev. B* **77**, 165104 (2008).
- [64] E. Fermi, *Rend. Accad. Naz. Lincei.* **6**, 602 (1927).
- [65] L. H. Thomas, *Proc. Cambridge Philos. Soc.* **23**, 542 (1927).
- [66] W. Brandt and M. Kitagawa, *Phys. Rev. B* **25**, 5631 (1982).
- [67] S.-M. Li, F. Mao, X.-D. Zhao, B.-S. Li, W.-Q. Jin, W.-Q. Zuo, F. Wang, and F.-S. Zhang, *Phys. Rev. B* **104**, 214104 (2021).
- [68] J. I. Fuks, P. Elliott, A. Rubio, and N. T. Maitra, *J. Phys. Chem. Lett.* **4**, 735 (2013).
- [69] C.-W. Lee, J. A. Stewart, R. Dingreville, S. M. Foiles, and A. Schleife, *Phys. Rev. B* **102**, 024107 (2020).

*Correction:* The penultimate sentence of the sixth paragraph in the Introduction contained a typographical error and has been fixed.

*Second Correction:* The final numerical value for the Fermi wave vector in the second complete sentence after Eq. (4) contained an error and has been fixed. The two threshold velocity values in the sentence following were erroneous and have been fixed.